■ **Non-Covalent Interactions** |*Hot Paper*|

London Dispersion and Hydrogen-Bonding Interactions in Bulky Molecules: The Case of Diadamantyl Ether Complexes

María Mar Quesada Moreno+,[a, b] Pablo Pinacho+,[a, b] Cristóbal Pérez,[a, b] Marina Šekutor,[c] Peter R. Schreiner,[c] and Melanie Schnell*[a, b]

Abstract: Diadamantyl ether (DAE, $C_{20}H_{30}O$) represents a good model to study the interplay between London dispersion and hydrogen-bond interactions. By using broadband rotational spectroscopy, an accurate experimental structure of the diadamantyl ether monomer is obtained and its aggregates with water and a variety of aliphatic alcohols of increasing size are analyzed. In the monomer, $C-H\cdots H-C$ London dispersion attractions between the two adamantyl subunits further stabilize its structure. Water and the alcohol partners bind to diadamantyl ether through hydrogen bonding and non-covalent $O_{water/alcohol}\cdots H-C_{DAE}$ and $C-H_{alcohol}\cdots H-C_{DAE}$ interactions. Electrostatic contributions drive the stabilization of all the complexes, whereas London dispersion interactions become more pronounced with increasing size of the alcohol. Complexes with dominant dispersion contributions are significantly higher in energy and were not observed in the experiment. The results presented herein shed light on the first steps of microsolvation and aggregation of molecular complexes with London dispersion energy donor (DED) groups and the kind of interactions that control them.

Introduction

Hydrogen bonding and dispersion interactions are key players in many chemical processes. Hydrogen bonding is essential to water's life-providing properties,[1] and its role in protein folding and chemical recognition is crucial.[2, 3] London dispersion (LD) interactions refer to the attractive term of the van der Waals equation.[4, 5] They are weak if only one pair of interactions is considered. However, their effect is pairwise additive and increases rapidly with system size and therefore faster than the number of atoms.[5] For example, the LD contributions were estimated to exceed 125.5 kJ mol^{-1} (30 kcal mol^{-1}, about one third of a covalent C—C single bond) in diamondoid

dimers.[6,7] While hydrogen bonding is known to be a rather directed interaction, this is less the case for dispersion. Nevertheless, it was found that in hydrogen-bonded complexes, LD interactions can largely influence the preferred structures.[8] As such, systematic studies of molecular complexes, where both hydrogen bonding and LD interactions can form, are powerful tools to study the relative contributions of hydrogen bonding and LD to molecular interactions.[9–13]

For example, two systematic analyses of aggregates of diphenyl ether (DPE)[14] and dibenzofuran (DBF)[15] with alcohols of increasing side-chain length were recently carried out. These studies provide valuable insights into the relationship of LD interactions and structural flexibility. Systematic investigations on the interplay between dispersion and hydrogen-bonding interactions in model systems reveal trends that can be extended to much larger molecular systems, for which the accurate structural determination is nowadays still unreachable with the available theoretical and experimental methods. As such, they can be helpful in predicting molecular aggregation and recognition processes.[16, 17]

Diadamantyl ether (DAE, $C_{20}H_{30}O$) represents a good model to study this interplay between LD and hydrogen-bonding interactions. DAE has two bulky adamantyl moieties linked by an ether group, which can act as an LD energy donor (DED)[5, 18] and hydrogen-bond acceptor. The ether oxygen is more shielded than in DPE and DBF owing to the bulkiness of the adamantyl moieties. This last feature makes it difficult to predict the preferred binding site—the adamantyl cages or the shielded oxygen atom.

In this study, we use high-resolution chirped-pulse Fourier transform microwave (CP-FTMW) spectroscopy from 2 to

[a] *Dr. M. M. Quesada Moreno,+ Dr. P. Pinacho,+ Dr. C. Pérez,*
Prof. Dr. M. Schnell
Deutsches Elektronen-Synchrotron, Notkestr. 85, 22607 Hamburg (Germany)
E-mail: melanie.schnell@desy.de

[b] *Dr. M. M. Quesada Moreno,+ Dr. P. Pinacho,+ Dr. C. Pérez,*
Prof. Dr. M. Schnell
Institute of Physical Chemistry, Christian-Albrechts-Universität zu Kiel
Max-Eyth-Str. 1, 24118 Kiel (Germany)

[c] *Dr. M. Šekutor, Prof. Dr. P. R. Schreiner*
Institute of Organic Chemistry, Justus Liebig University
Heinrich-Buff-Ring 17, 35392 Giessen (Germany)

[+] *These authors contributed equally to this work.*

💻 *Supporting information and the ORCID identification number(s) for the*
ⓘ *author(s) of this article can be found under:*
https://doi.org/10.1002/chem.202001444.

Chemistry–A European Journal

Full Paper
doi.org/10.1002/chem.202001444

Chemistry Europe
European Chemical
Societies Publishing

8 GHz.[19, 20] Quantum-chemical computations aid the analysis of the experimental data. With rotational spectroscopy in hand, structurally similar molecules like diastereomers, isotopologues, conformers, and structural isomers can be observed and unambiguously differentiated as they present unique rotational spectra.[21–24] We report the structure of DAE itself as well as the preferred binding sites and an analysis of the intermolecular interactions taking place between DAE and water as well as two alcohols with different sizes and steric complexity, namely ethanol (EtOH) and *tert*-butanol (*t*BuOH). Their structures are studied in the gas phase under the cold and isolated conditions of a supersonic expansion. In this way, we can analyze the intrinsic structures of complexes in a solvent-free environment.

Results and Discussion

The broadband rotational spectrum of the DAE monomer is shown in Figure S1 in the Supporting Information, and its experimental rotational constants resulting from a recurrent fit of the rotational transitions by using an asymmetric-top Hamiltonian (see Experimental Section and Computational Details) are collected in Table 1. The DAE monomer showed only *b*-type rotational transitions, thus pointing to a sizeable μ_b dipole-moment component and vanishing μ_a and μ_c values. The high sensitivity and resolution of this technique often allows the observation of isotopically substituted species in natural abundance. For the DAE monomer, the strongest rotational transitions had a signal-to-noise ratio (SNR, from the five most intense transitions) of approximately 700:1, which allowed the simultaneous observation of the spectra of all ten singly substituted ^{13}C and one ^{18}O isotopologues in natural abundance. Their respective experimentally determined rotational constants are summarized in Table S1 in the Supporting Information. The DAE monomer has C_2 symmetry, with the C_2 axis coinciding with the *b* inertial axis. Owing to this symmetry, the recorded microwave spectrum presents only ten different spectra with double intensity (instead of twenty) arising from single ^{13}C and one from ^{18}O substitution.

Structure determination from experimental isotopic data is typically performed with two different approaches. The Kraitchman method is based on the changes in the moments of inertia with isotopic substitution (assuming that the bond lengths do not change upon substitution). Solving the Kraitchman equations[25] gives the atom coordinates for the substituted atom in the principal inertia axis system and allows building the so-called substitution structure, r_s, atom by atom. This method "locates" the atoms within the molecular frame, but presents several drawbacks. For atoms near the principal axes, it may give very small or even imaginary values for the coordinates, which reduces its accuracy. Also, the Kraitchman equations only provide the absolute values of the coordinates, whereas the signs must be obtained from quantum-chemical computations or/and chemical intuition. In the other method, a least-squares fit of certain atom distances and angles is performed[26] to reproduce all the experimental moments of inertia in a particular vibrational state. The simplest geometry is that of the vibronic ground state, r_0.[27]

The r_0 and r_s experimental structures for DAE were determined by exploiting the fitted rotational constants of the singly substituted ^{13}C and ^{18}O species. They are summarized in Table S2 in the Supporting Information. Quantum-chemical computations give us the equilibrium structure, r_e. In Figure 1, a comparison between this computed r_e and the experimental r_0 structures is displayed, showing good agreement. For DAE, the inclusion of correction terms accounting for molecular vibrations, which lead to the $r_m^{(1)}$ structure,[28] does not improve the least-squares fit. This indicates that diadamantyl ether is rather rigid, and vibration–rotation effects are negligible. This rigidity is also supported by the fact that centrifugal distortion constants were not needed for fitting the DAE monomer (Table 1).

In a second set of experiments, we recorded the rotational spectra of DAE–water (DAE-w), DAE–EtOH, and DAE–*t*BuOH clusters (see the Experimental Section for details). Parts of the experimental spectra are shown in the top traces of Figure 2, whereas the bottom traces correspond to simulations based on an asymmetric-top Hamiltonian using the experimentally determined rotational parameters for the complexes. These ex-

Table 1. Experimental spectroscopic constants of the DAE monomer and the observed DAE-*n*w clusters.

	DAE	DAE-1w	DAE-2wa	DAE-2wb	DAE-3w
A [MHz][a]	822.35342(11)[e]	587.018803(90)	446.45475(17)	438.85323(12)	332.49466(22)
B [MHz]	188.429111(22)	188.009580(35)	182.439093(52)	177.610322(46)	173.70380(35)
C [MHz]	187.382764(23)	171.836814(38)	159.580761(56)	150.684238(44)	137.55366(33)
Δ_J [kHz]	–	0.001028(61)	0.00130(10)	0.001333(52)	–
Δ_{JK} [kHz]	–	–	0.0272(10)	0.01891(73)	0.0526(13)
Δ_K [kHz]	–	0.0222(10)	–	–	–
δ_K [kHz]	–	–	–	–	−0.119(15)
$a/b/c$[b]	n/y/n	y/y/y	y/y/y	y/y/n	n/n/y
N[c]	152	608	325	323	84
σ [kHz][d]	5.7	6.6	6.6	6.5	6.9

[a] A, B, and C are the rotational constants; Δ_J, Δ_{JK}, Δ_K, and δ_K are the quartic centrifugal distortion constants. [b] a, b, and c are the type of transitions observed (n: not observed, y: observed). [c] N is the number of fitted transitions. [d] σ is the root-mean square deviation of the fit. [e] Standard error in parentheses in units of the last digit.

Chemistry–A European Journal

Full Paper
doi.org/10.1002/chem.202001444

Chemistry Europe
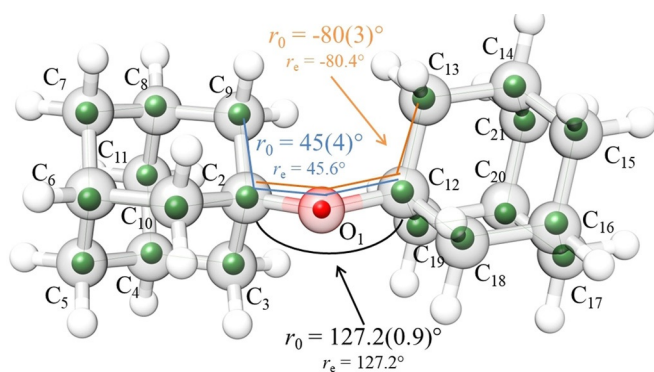European Chemical
Societies Publishing

Figure 1. Experimentally determined r_0 structure (green spheres for carbon and red for oxygen) and computed one (r_e, underlying structure, B3LYP-D3(BJ)/def2-TZVP) for the DAE monomer. Experimentally determined bond lengths are summarized in Table S3 in the Supporting Information.

Table 2. Experimental spectroscopic constants of the DAE-EtOH$_g$, DAE-EtOH$_t$, and DAE-tBuOH complexes.

	DAE-EtOH$_t$	DAE-EtOH$_g$	DAE-tBuOH
A [MHz][a]	322.16621(14)[e]	353.97815(11)	234.786175(54)
B [MHz]	186.739005(49)	185.025105(34)	180.632992(32)
C [MHz]	138.506018(63)	145.393198(43)	119.278830(39)
Δ_J [kHz]	0.000744(65)	0.000809(52)	0.000631(50)
Δ_{JK} [kHz]	0.03608(63)	0.01873(51)	0.01578(29)
Δ_K [kHz]	−0.01825(89)	–	−0.00609(30)
δ_K [kHz]	0.01141(93)	–	0.00393(22)
$a/b/c$[b]	n/y/y	y/y/y	y/y/y
N[c]	275	561	623
σ [kHz][d]	6.4	7.4	5.0

[a] A, B, and C are the rotational constants; Δ_J, Δ_{JK}, Δ_K, and δ_K are the quartic centrifugal distortion constants. [b] a, b, and c are the type of transitions observed (n: not observed, y: observed). [c] N is the number of fitted transitions. [d] σ is the root-mean square deviation of the fit. [e] Standard error in parentheses in units of the last digit.

perimental rotational constants are summarized in Table 1 and Table 2.

The DAE–water spectrum presents a high density of lines (Figure 2 a and b), indicating the presence of several DAE-nw (n = 1–3) clusters. We identified one DAE-1w complex, which exhibited mainly a b-type rotational spectrum. The signal-to-noise ratio (SNR) of the strongest transitions was about 85:1, comparable to the one of the DAE monomer (94:1) in this DAE–water rotational spectrum. Two complexes with two water molecules (DAE-2wa and DAE-2wb) and one complex with three water molecules (DAE-3w) complexed to diadamantyl ether were also identified. DAE-2wa and DAE-2wb showed

respective SNR values of approximately 17:1 and 6:1, whereas the DAE-3w complex spectrum was significantly weaker with a SNR of roughly 3:1. Assignment of these species was guided by comparing the experimental rotational constants and the type of rotational transitions with the information obtained from quantum-chemical computations. A conformational search was performed by using the GFN-xTB program.[29, 30] The most favorable structures were further optimized by employing the B3LYP-D3(BJ)/def2-TZVP level of theory (see Experimental and Computational Sections for details).
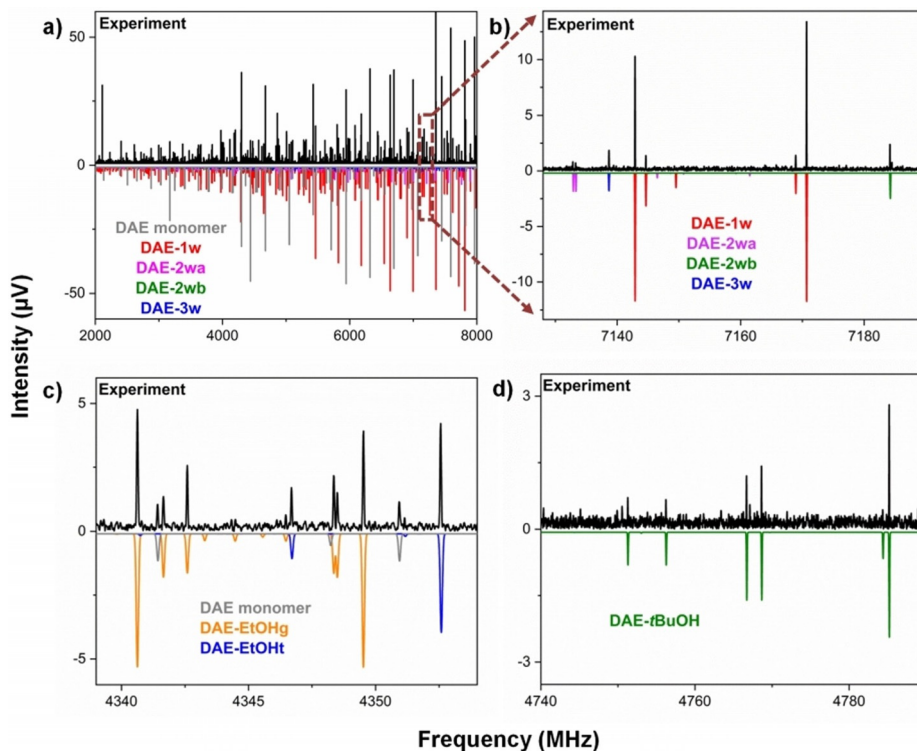

Figure 2. Sections of the broadband rotational spectra of a,b) DAE-nw (n = 1–3), c) DAE-EtOH, and d) DAE-tBuOH complexes. The upper traces depict the experimental spectra, whereas the lower traces are simulations of the experimentally identified complexes (rotational temperatures of 1 K) based on fitted rotational parameters.

Chemistry–A European Journal

Full Paper
doi.org/10.1002/chem.202001444

Chemistry Europe
European Chemical
Societies Publishing

Quantum-chemical computations provided two DAE-1w minima, with an energy difference of 22.2 kJ mol^{-1}. In the higher-energy one (DAE-1w(II)), the water molecule binds to one adamantyl moiety and not to the ether oxygen atom; it is too high in energy to be sufficiently populated. By comparing the theoretical and experimental values of the A, B, and C rotational constants, we can unambiguously assign the theoretical DAE-1w(I) structure to the experimentally identified DAE-1w (Table 1, Table S5 and Figure S2 in the Supporting Information). In this DAE-1w(I) complex, the water molecule binds to the ether oxygen through a strong O—H···O hydrogen bond, with a computed O—H distance of 1.89 Å and an O—H···O angle around 172.0°. In addition, rather short C—H···O distances of neighboring methylene groups with the water (C—H···O distances of about 2.65 Å, Figure 3) indicate the presence of LD interactions as further revealed by non-covalent interaction (NCI) computations (see below).

The conformational landscape of DAE-2w is richer. Four DAE-2w structures with relative energies below 3.2 kJ mol^{-1} were identified as minima (B3LYP-D3(BJ)/def2-TZVP, Table S6 and Figure S3 in the Supporting Information). 2w(I) (0.0 kJ mol^{-1}) and 2w(II) (1.5 kJ mol^{-1}) are the lowest-energy isomers, whereas 2w(III) (2.9 kJ mol^{-1}) and 2w(IV) (3.2 kJ mol^{-1}) are higher in energy. The only difference between 2w(I) and 2w(III) is the arrangement of the hydrogen atoms in the water molecules. The same difference is observed between 2w(II) and 2w(IV). Their computed rotational constants are similar, which complicates an assignment based on the rotational constants alone. Comparison of the experimental and computed B and C rotational constants shows a correlation between species 2wa with 2w(I) or 2w(III) and 2wb with 2w(II) or 2w(IV). The fact that we only observe two DAE-2w complexes experimentally instead of four points to low relaxation barriers between 2w(I)–2w(III) and 2w(II)–2w(IV), respectively. In addition, several c-type rotational transitions were observed for the 2wa complex but not for 2wb. This fact is in good agreement with the theoretical results, which gave a larger theoretical μ_c value for the 2w(I) complex than for 2w(II) (0.48 D vs. 0.06 D). This reinforces the assignment of the experimentally observed 2wa and 2wb complexes as the calculated 2w(I) and 2w(II), respectively (Figure 3).

From a structural point of view, both 2wa and 2wb maintain the structural feature of DAE-1w, with a rather strong hydrogen bond between one water molecule and the ether oxygen atom. The corresponding O—H···O bond lengths and angles characterizing this hydrogen bond are 1.86 Å/169.0° and 1.84 Å/174.7° for DAE-2wa and DAE-2wb, respectively. The second water molecule forms a hydrogen bond to the first H$_2$O with additional bonds to one of the closest pockets consisting of three methylene groups in the diadamantyl moieties (Figure 3 and Figure S3 in the Supporting Information). For DAE-2wa and -2wb, this additional binding occurs to the two different adamantyl moieties, respectively (Figure 3).

The exploration of the shallow potential energy surface (PES) for DAE-3w rendered nine possible isomers (Figures S4 and S5 in the Supporting Information) with relative energies within 2.8 kJ mol^{-1} (Table S7 in the Supporting Information). In all of them, the three water molecules are anchored to DAE
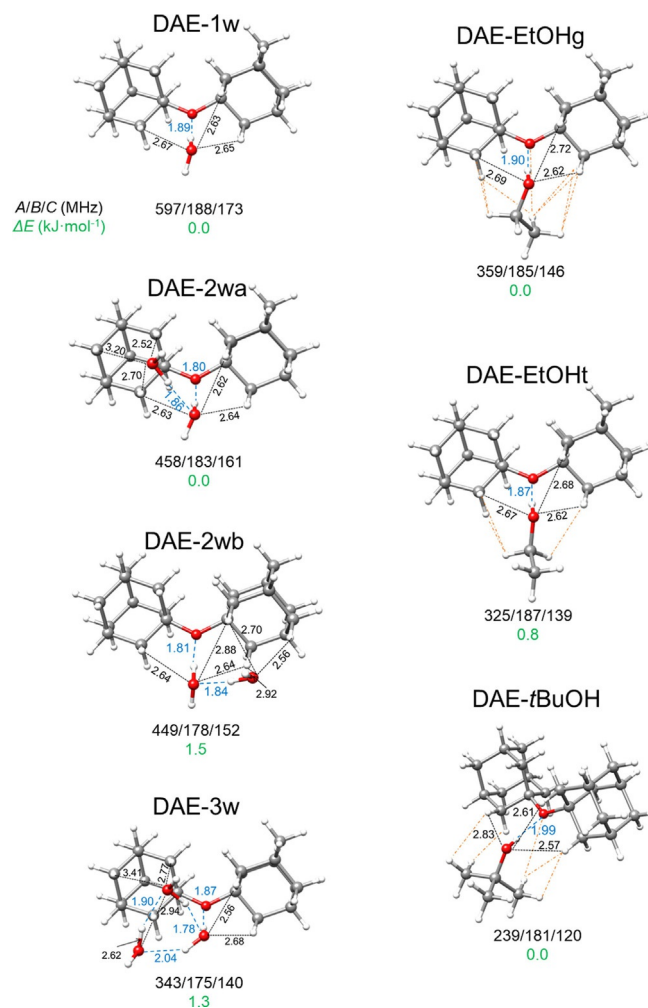

Figure 3. Molecular structures of the DAE-nw (1–3), DAE-EtOH, and DAE-tBuOH clusters optimized at the B3LYP-D3(BJ)/def2-TZVP level of theory, labeled according to the experimentally identified complexes (Tables S5–S7, S9–S10, and Figures S2–S7 in the Supporting Information). They correspond to the DAE-1w(I), DAE-2w(I), DAE-2w(II), DAE-3w(V), DAE-EtOH(I), DAE-EtOH(II), and DAE-tBuOH(I) theoretical structures. The theoretical O—H···O and C—H···O distances are given in Å. The zero-point corrected relative energies (ΔE, kJ mol^{-1}) are calculated with respect to the most stable minimum of each species.

through an O—H···O hydrogen bond and C—H···O interactions. One of the water molecules is located in the middle of the dispersive pocket created by the three closest methylene groups of the diadamantyl moieties in the 3w(I), 3w(II), 3w(III), 3w(IV), 3w(VI), and 3w(VIII) complexes (Figure S5 in the Supporting Information).

The DAE-3w structures can be grouped according to the arrangement of the three water molecules: 1) keeping a cyclic configuration like in the isolated water trimer[31] or 2) forming an open chain. All DAE-3w isomers below 1.4 kJ mol^{-1} (from DAE-3w(I) to DAE-3w(VI)) as well as DAE-3w(VIII) are included in group 1, whereas DAE-3w(VII) and DAE-3w(IX) constitute group 2. Interestingly, the water molecule arrangements of DAE-2wa and -2wb, respectively, are contained in the DAE-3w structures: The DAE-2wa for 3w(V), 3w(VII), and 3w(IX) and the DAE-2wb for 3w(I) to 3w(IV), 3w(VI), and 3w(VIII).

Chemistry–A European Journal

Full Paper
doi.org/10.1002/chem.202001444

Chemistry Europe
European Chemical
Societies Publishing

The structural difference between some of these isomers, like the pairs 3w(I)–3w(IV) and 3w(II)–3w(VI), respectively, is just a small change in the arrangement of one of the water molecules. All these structures were tested to be real minima by checking for imaginary frequencies. In this respect, it is also interesting to point out that DAE-3w(I) and DAE-3w(II) keep the same arrangement for their heavy atoms, but differ in the clockwise and counterclockwise orientations for the water trimer structure. This is also the case for DAE-3w(IV) (clockwise) and DAE-3w(VI) (counterclockwise) (Figures S4 and S5 in the Supporting Information). The same phenomenon was observed in other molecule–3w clusters where the water molecules form a cyclic arrangement.[32]

As mentioned, only one DAE-3w complex was spectroscopically observed under the cold conditions of our molecular jet, showing a c-type spectrum (Table 1). The different orientations of the three water molecules cause only small changes in the mass distribution because of the overall large mass of the complex. For this reason, the rotational constants for all the calculated DAE-3w structures are similar. However, their electric charge distributions change for the different water arrangements (Table S7 in the Supporting Information). For DAE-3w(VII), for example, the μ_c dipole moment component is predicted to be close to zero, so no c-type transitions are expected. In the case of DAE-3w(I), DAE-3w(II), and DAE-3w (IX), b-type rotational transitions should be the strongest ones. Thus, these isomers can be discarded from being the experimentally identified structure. The five remaining isomers are predicted to have a c-type rotational spectrum, and all of them are lower than 1.4 kJ mol⁻¹ (apart from DAE-3w(VIII), which is predicted to have a relative energy of 2.7 kJ mol⁻¹). Reoptimization of these five isomers with a strong c-type spectrum at the MP2/aug-cc-pVTZ level (not ZPVE corrected) resulted in the DAE-3w(V) isomer as the lowest-energy cluster. As ZPVE corrections at the MP2/aug-cc-pVTZ level were computationally too demanding for these large weakly bound complexes, we chose to add the B3LYP-D3 ZPVE corrections to the MP2 energies. This generated the same energy order (see Table S8 in the Supporting Information). Additionally, DAE-3w(V) is the isomer with the largest μ_c dipole moment component, which supports the fact that only c-type rotational transitions are observed for the experimentally identified DAE-3w complex. The difference between its rotational constants, $B-C$ (35.1 MHz), is also the closest to that of the experimental isomer (36.2 MHz). Note that differences between rotational constants are often determined more accurately by quantum-chemical computations than absolute values.[21]

Considering that the DAE-3w cluster is significantly weaker than the 1w and 2w clusters, it is not surprising that only one cluster was observed despite the rather large number of nine predicted low-energy clusters. Although the global minimum structure is supposed to be the most populated one under supersonic-jet conditions, the strengths of rotational transitions also depend on the square of the respective dipole moment component μ_i. Especially in the presence of several low-energy structures together with an overall low intensity of the spectrum, a high-energy structure with a large dipole moment

component could exhibit a stronger spectrum than the global minimum and thus be the only one observed. These difficulties in assigning a structure to the observed DAE-3w spectrum illustrate the challenges that such weakly bound clusters where (several) light molecules (like H₂O) are bound to a heavy molecule (like DAE) pose for both high-resolution rotationally resolved spectroscopy and quantum-chemical computations. Even though an exact structure determination including the arrangement of the water hydrogen atoms is not possible, we can still conclude that the observed structure exhibits a cyclic water trimer arrangement.

In the DAE–water complexes, the average $O_{DAE}\cdots O_w$ distance changes with cluster size: 2.86 Å (DAE-1w), 2.80 Å (DAE-2wa and DAE-2wb), and 2.81 Å (DAE-3w). This initial shortening can be ascribed to hydrogen bond cooperativity, which has been observed in progressively larger cyclic water clusters[33] and in other systems like formamide₂–water,[34] acenaphthene–water,[32] camphor–water,[35] or β-propiolactone–water.[36] For the 3w cluster, an anticooperative effect may counteract the cooperativity, which is indicated by a slight increase of the $O_{DAE}\cdots O_w$ distance. This anticooperativity can arise from the double donor role of one water molecule. The O⋯O distances of the DAE-1w, DAE-2w, and DAE-3w clusters are comparable to those of the water trimer (2.85 Å),[31] and significantly shorter than those of the water dimer (2.98 Å).[37]

Figure 3 shows that the cyclic water trimer is distorted for DAE-3w, as the hydrogen-bond distances between the water molecules are different (Figures 3 and S8 in the Supporting Information). The symmetry-adapted perturbation theory (SAPT(0)) results presented below show that the LD contributions are higher in the DAE-3w complex than in the DAE-1w and DAE-2w clusters, which is supported by the NCI computations (see below), which reveal attractive interactions between DAE and the three water molecules. A distorted cyclic water trimer structure was also observed on the surface of the polycyclic aromatic hydrocarbon acenaphthene.[32]

The analysis of the DAE–EtOH and DAE–tBuOH spectra results in two DAE–EtOH clusters and one DAE–tBuOH complex, respectively. Parts of their experimental spectra are shown in panels c) and d) of Figure 2 as the top black trace. Although for the ethanol monomer the trans form (EtOH_t) is more stable than the gauche conformer (EtOH_g),[38] both species are observed in complexes. A preference for the EtOH_g conformer is observed for complexes where ethanol interacts with partners through additional weak attractive interactions next to the hydrogen bond.[39–45] In the acetone–EtOH system, for example, only the EtOH gauche complex was observed, which was attributed to relaxation processes between the trans and the gauche complexes.[46] In the NH₃–EtOH complex, where no secondary interactions take place, the trans isomer was more populated than NH₃–EtOH gauche.[47]

In the case of DAE–EtOH, one of the observed isomers could unambiguously be assigned to a complex with trans EtOH (DAE-EtOH_t; Figure 3), namely DAE-EtOH(II) from our computations (Table S9 in the Supporting Information), owing to the good agreement between the experimental and computed A, B, and C rotational constants. The structures of the experimen-

Chemistry–A European Journal

Full Paper
doi.org/10.1002/chem.202001444

Chemistry Europe
European Chemical
Societies Publishing

tally observed isomers are shown in Figure 3, with their rotational constants summarized in Table 2.

The rotational constants of the second experimentally observed complex agree with several calculated DAE–EtOH clusters (DAE-EtOH(I), DAE-EtOH(III), and DAE-EtOH(IV)), which all host EtOH in its *gauche* form (DAE-EtOH$_g$; Table S9 and Figure S6 in the Supporting Information). Experimentally, we observed *a*-, *b*-, and *c*-type rotational transitions, which allows us to discard the DAE-EtOH(III) isomer owing to its low computed μ_a value. The computed B and C rotational constants for DAE-EtOH(I) and DAE-EtOH(IV) agree well with the experimental ones. However, the experimental value of the A rotational constant and the relative intensities of the *a*-, *b*-, and *c*-type transitions, which provide information of the relative ordering of μ_a, μ_b, and μ_c, agree better with those of DAE-EtOH(I). Furthermore, DAE-EtOH(I) (Figure 3) is predicted as the lowest-energy isomer.

Overall, the spectra of DAE-EtOH$_g$ show more intense transitions than DAE-EtOH$_t$ (SNR of about 22:1 and 11:1, respectively), indicating a higher population in the supersonic expansion considering the dipole moment components (Table S9 in the Supporting Information).

Finally, only one DAE-*t*BuOH complex was observed in our experiments (Figure 2 d and Figure 3), and there is no indication of further isomers in the spectrum. Quantum-chemical computations predict three DAE-*t*BuOH isomers to be lower in energy than 3.1 kJ mol^{-1}. They differ in the *t*BuOH orientation within the complex (Table S10 and Figure S7 in the Supporting Information), with *t*BuOH being anchored to DAE through an O—H$_{tBuOH}$···O$_{DAE}$ hydrogen bond, supported by LD interactions (O$_{tBuOH}$···H—C$_{DAE}$, C—H$_{tBuOH}$···O$_{DAE}$, and C—H$_{tBuOH}$···H—C$_{DAE}$).

All computed DAE-*t*BuOH complexes ((I)–(III)) have similar rotational constants. Once again, the experimental dipole moment components μ_a, μ_b, and μ_c provide us with additional information. In the identified complex, we deduced an approximate ordering of $\mu_b > \mu_a \approx \mu_c$ from the strengths of the different rotational transitions. This supports the assignment of the experimental DAE-*t*BuOH complex as DAE-*t*BuOH(I), as in DAE-*t*BuOH(II) *a*-type rotational transitions should be weaker than *c*-type ($\mu_b > \mu_c > \mu_a$). DAE-*t*BuOH(III) is higher in energy (3.1 kJ mol^{-1}), and also its computed dipole moment components do not agree with the experimental ones ($\mu_a \approx \mu_b > \mu_c$). It is interesting to note that three further DAE-*t*BuOH complexes without O—H···O hydrogen bonding are predicted to be 12.0, 13.9, and 15.1 kJ mol^{-1} higher in energy. Although this is certainly too high to be relevant for our study employing supersonic-jet cooling, this value is significantly lower than what we computed for the non-O—H···O complexes of DAE-EtOH (21 kJ mol^{-1}).

Note that the structure of DAE is the same in all complexes. This can be rationalized by comparing the C9-C2-O1-C12 dihedral angle (see Figure 1 for the labeling) in the DAE–alcohol clusters, the value of which is about 48° (Table S11 in the Supporting Information) in all of them. The interactions of the different alcohols with increasing alkyl group size through the DAE ether oxygen and the hydrogens of the methylene groups thus do not change this angle owing to the rigid bulk-

iness of DAE itself. This is contrary to the DPE complexes, where the relative arrangement of the phenyl rings with respect to each other changes to maximize the interaction with the respective alcohols.[14]

We applied non-covalent interaction (NCI) analyses to visualize and characterize the different interactions present in the DAE complexes as hydrogen bonds (strong attraction, blue color), LD non-covalent interactions (green color), and steric congestion (strong repulsion, red color) interactions.[48] This method investigates the electron density regions in which the reduced density gradient (RDG) vanishes at low electron densities. The RDG function is essentially a dimensionless form of the electron density gradient norm function.[48] An NCI analysis provides chemically intuitive iso-surfaces of the RDG. The sign of the second Hessian eigenvalue (λ_2) of the density allows us to distinguish between different types of non-covalent interactions. The strength of the interaction can be derived from the electron density ρ in the corresponding region (Figures 4 and S8 in the Supporting Information).

The NCI plots show the existence of attractive interactions between the hydrogen atoms of the methylene groups of the two different adamantyl subunits in the DAE monomer (Figure 4). In DAE-EtOH and DAE-*t*BuOH, the alkyl groups of EtOH and *t*BuOH and the methylene groups of DAE also interact through C—H···H—C interactions, which are characterized as attractive by the NCI analysis. This is especially clear in the DAE-EtOH$_g$ and DAE-*t*BuOH complexes, where there are more C—H···H—C contacts than in the DAE-EtOH$_t$ complex (Figure 3 and Figure 4). The existence of these C—H···H—C interactions could explain why the O—H···O hydrogen bond length is longer in the DAE-*t*BuOH complex (1.99 Å) than in the DAE-1w (1.89 Å), DAE-EtOH$_t$ (1.87 Å), and DAE-EtOH$_g$ (1.90 Å) complexes. The *t*BuOH group arranges in a way such that its methyl groups interact with the methylene groups of DAE through LD interactions and force the hydroxyl group of *t*BuOH to be located somewhat more distant from the DAE oxygen.
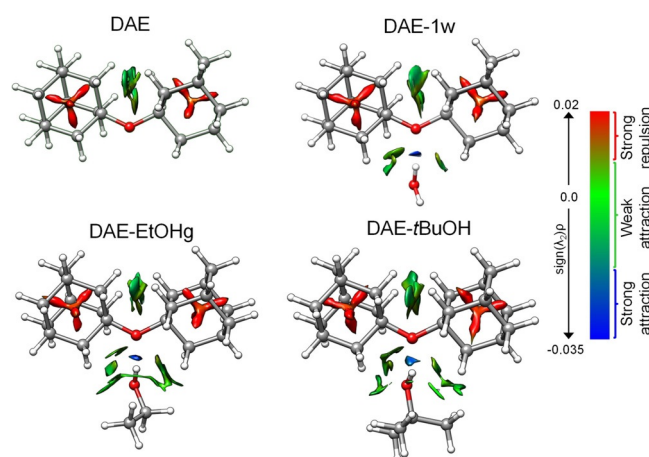

Figure 4. Non-covalent interaction (NCI) analysis for the DAE monomer and the lowest-energy DAE-1w, DAE-EtOH$_g$, and DAE-*t*BuOH complexes. Blue color represents strong attractive interactions, green shows weak attractive interactions, such as dispersion, and red indicates repulsive interactions.

Chemistry–A European Journal

Full Paper
doi.org/10.1002/chem.202001444

Chemistry Europe
European Chemical
Societies Publishing

To verify this, we computed the rotational constants of DAE-tBuOH for different O—H···O distances, with the other parameters being fixed. Table S12 (in the Supporting Information) shows that the A rotational constant changes for different O—H···O distances and adopts a rather large value (247.0 MHz) when the O—H···O length is 1.85 Å. However, the A value is 239.3–233.6 MHz for elongated distances of 1.98–2.08 Å, which is closer to the experimentally determined A rotational constant (234.786175(54) MHz).

A more quantitative understanding of the chemical nature of the non-covalent interactions can be provided by using symmetry-adapted perturbation theory (SAPT).[49] SAPT(0)/jun-cc-pVDZ computations give the different binding contributions in each of the DAE complexes: electrostatics, induction, LD, and exchange (Figure 5 and Tables S13 and S14 in the Supporting Information). The results were compared with those of DME (EtOH$_g$ and EtOH$_t$, see the Supporting Information),[41] DPE (tBuOH (O—H···O and O—H···π motifs for both)),[14] and DBF (tBuOH (O—H···π))[15] complexes. The DPE, DBF, and DAE monomers themselves exhibit some similarities. DPE has two phenyl rings linked by an ether group and is flexible, whereas in DAE the phenyl rings are exchanged with two bulky adamantyl moieties. In DBF, the two phenyl rings are linked by an additional bond, making its structure rigid and planar.

In DAE, the ether oxygen is less accessible than in DPE and DBF owing to the bulkiness of the adamantyl moieties. In the DPE complexes,[14] an overall stabilization of the OH···O motif with increasing side-chain size in comparison with the OH···π motif was observed because for the larger alcohols the O—H···O structure also allows for stabilization via dispersion with the phenyl rings. The trend observed in the DBF study is completely reversed,[15] with a preference for the OH···π over the OH···O interaction with increasing alkyl-group size. Detailed explanations of these preferences for DPE and DBF can be found in Refs. [14] and [15], respectively. The DAE and DPE complexes exhibit the O—H···O motif also for larger, more bulky binding partners because their respective adamantyl or phenyl rings can establish secondary interactions. However, this cannot be achieved in the DBF-tBuOH complex because of its planarity.

The total SAPT interaction energy is similar for all the 1:1 DAE complexes, presenting a slightly lower value for DAE-1w. In the DAE complexes, the electrostatic interactions are the dominant attractive components, although LD contributions increase according to the size of the alcohol partner (Figure 5). Expectedly, their value is particularly high in the DAE-EtOH$_g$ and DAE-tBuOH complexes, which have more C—H···H—C contributions. The largest LD contribution is reached in the DAE-tBuOH complex, where the sum of LD and induction is comparable to the electrostatic contributions. In the DPE-tBuOH (O—H···O and O—H···π) complexes, electrostatics and LD interactions contribute equally, as the aromatic rings and the alkyl groups act as DEDs. LD interactions play a crucial role becoming the most stabilizing contribution in the DBF-tBuOH (O—H···π) cluster.[15] Note that the exchange-repulsion energy values are similar for all the DAE complexes.

Conclusion

We report a detailed structural study of the DAE molecule as well as the experimental and theoretical characterization of various DAE–water and –alcohol aggregates with increasing side-chain size of the alcohol. This work represents an accurate structural determination carried out for a rather large molecule (21 heavy atoms) by rotational spectroscopy. The DAE monomer is stabilized by LD interactions between the two adamantyl subunits. In the DAE–alcohol clusters, DAE acts as both hydrogen-bond acceptor and dispersion "host" because of its ether and bulky adamantyl groups, where the alcohols with increasingly large side-chain groups can be anchored. Non-hydrogen-bonded clusters were not observed and are predicted to have much higher relative energies.

The structure of the isolated DAE molecule and when it is complexed with the different alcohols remains essentially unchanged, showing its rigid and bulky character. LD interactions also take place between the hydrogens of the alkyl groups of EtOH and tBuOH partners and those of DAE, so that an elongation of the O—H···O hydrogen-bond in DAE–tBuOH is observed. As mentioned in the introduction, LD interactions accumulate in increasingly larger molecular systems and eventually become the dominant contribution.[5]

We also illustrate the first steps towards the formation of the DAE solvation shell involving up to three molecules of water, which shows cooperative and anticooperative effects. Our systematic study can help understand the interplay between LD and hydrogen-bonding interactions in the formation
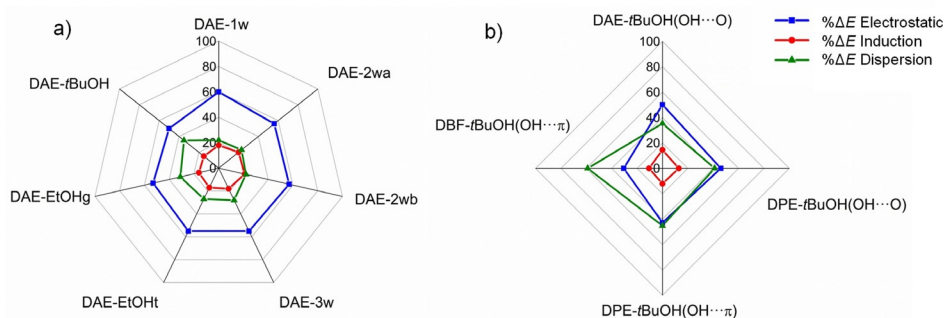

Figure 5. Radar charts showing the attractive contributions obtained from SAPT(0) computations as a percentage of the overall attractive interactions for DAE complexes in comparison to related tBuOH complexes. Electrostatics, induction, and dispersion contributions are shown in blue, red, and green, respectively.

Chemistry–A European Journal

Full Paper
doi.org/10.1002/chem.202001444

Chemistry Europe
European Chemical
Societies Publishing

and stabilization of bulky complexes as well as their (micro-)solvation processes. Not only is characterizing these forces important for chemical synthesis and reactivity, but also for the construction of new materials. This work leads the way to the structural study of larger size bulky complexes where LD interactions play a key role.

Experimental Section and Computational Details

Synthesis of diadamantyl ether (DAE)
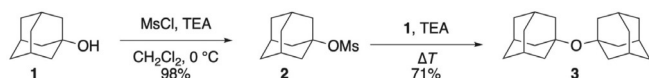
1-Adamantyl methanesulfonate[50] (**2**) was prepared by dissolving 1-hydroxyadamantane (**1**; 761 mg, 5 mmol) in CH_2Cl_2 (25 mL), and the reaction mixture was cooled with an ice bath. Then, triethyl-amine (TEA, 1 mL, 7.5 mmol) was added as well as methanesulfonyl chloride (MsCl, 0.43 mL, 5.5 mmol, dropwise). After stirring for 15 min the reaction mixture was extracted with water, washed with 5% H_2SO_4 (aq.) and Na_2CO_3 (sat., aq.). The organic phase was dried over Na_2SO_4, filtered, and evaporated, yielding **2** as a white solid (1.126 g, 98%). IR (KBr): $\nu = 3426$ (br), 2914 (s), 2851 (m), 1455 (w), 1358 (m), 1323 (s), 1173 (s), 1044 (m), 904 (s), 833 (m), 761 (w), 528 cm^{-1} (m); ^{1}H NMR (CDCl$_3$, 400 MHz): $\delta = 1.66$ (s, 6H), 2.23 (br s, 9H), 2.98 ppm (s, 3H, Me); ^{13}C NMR (CDCl$_3$, 100 MHz): $\delta = 31.5$ (CH, 3C), 35.6 (CH$_2$, 3C), 41.0 (CH$_3$, 1C), 43.0 (CH$_2$, 3C), 91.8 ppm (C, 1C, C-O); HRMS (ESI): calcd for [C$_{11}$H$_{18}$O$_3$SNa]$^+$: 253.0875; found: 253.0876.

1,1′-Diadamantyl ether[51] (**3**) was prepared by heating 1-adamantyl methanesulfonate (**2**; 2.303 g, 10 mmol), 1-hydroxyadamantane (**1**; 1.522 g, 10 mmol), and TEA (1.4 mL, 10 mmol) in a sealed tube at 80°C for 4 h.[52] The reaction mixture was dissolved in CH_2Cl_2, extracted with water, washed with 10% HCl (aq.) and NaHCO$_3$ (sat., aq.). The organic phase was dried over Na_2SO_4, filtered, and evaporated. The resulting crude product was purified by using column chromatography (CH_2Cl_2 as eluens), yielding **3** as a white solid (2.031 g, 71%). M.p.: 186–187°C. IR (KBr): $\nu = 3429$ (br), 2902 (s), 2849 (m), 1450 (w), 1350 (m), 1297 (w), 1117 (m), 1101 (w), 1086 (s), 990 (w), 819 cm^{-1} (w); ^{1}H NMR (CDCl$_3$, 400 MHz): $\delta = 1.55$–1.64 (m, 12H), 1.83–1.95 (m, 12H), 2.08 ppm (br s, 6H); ^{13}C NMR (CDCl$_3$, 100 MHz): $\delta = 31.1$ (CH, 6C), 36.5 (CH$_2$, 6C), 45.9 (CH$_2$, 6C), 74.2 ppm (C, 2C, C-O); HRMS (ESI): calcd for [C$_{20}$H$_{30}$ONa]$^+$: 309.2195; found: 309.2200.

Chirp pulse Fourier transform microwave (CP-FTMW) spectroscopy

All the broadband rotational spectra were recorded with the Hamburg broadband chirped-pulse Fourier-transform microwave (CP-FTMW) spectrometer COMPACT in the frequency range 2–8 GHz.[20] We used custom-made sample reservoirs for DAE as part of our pulsed valves, located close to the valve orifice and heated to 185°C to generate sufficient vapor pressure. Distilled water, ethanol, or *tert*-butanol was placed in a second reservoir located upstream outside the vacuum chamber, which was not heated. Neon was used as the carrier gas, with a backing pressure of 3 bar, and flowed over water, ethanol, or *tert*-butanol, respectively, and then through the heated reservoir containing DAE. We used a pulsed

valve (General valve Series 9) operated at 9 Hz to supersonically expand the molecules seeded in the carrier gas into the vacuum chamber, where it was polarized by a 4 µs long chirp spanning the 2–8 GHz frequency range. The microwave chirps were created by an arbitrary waveform generator (AWG), amplified with a 300 W traveling wave tube amplifier and then broadcast into the vacuum chamber by using a horn antenna. The molecular signal was collected in the time domain as a free induction decay (FID). Fast Fourier transformation of the FID resulted in the rotational spectrum in the frequency domain. The experimental setup is described in detail in ref. [20]. The "fast frame" option of the digital oscilloscope was used for these experiments.[53] Eight back-to-back excitation chirps were performed per gas pulse, and the subsequent eight FID acquisitions were co-added and averaged. In this way, the measurement time and sample consumption were decreased, resulting in an effective repetition rate of 72 Hz for the experiment. The FID was recorded for 40 µs, which generated a frequency resolution of 25 kHz in our Fourier transformed microwave spectrum. The number of FIDs that were co-added to obtain the final spectra was 3.5, 6.3, and 3.8 million for the DAE-w, DAE-EtOH, and DAE-*t*BuOH complexes, respectively. We did not observe any line splittings arising from internal dynamics in any experimental spectra. The interactions between the hydroxyl and alkyl groups of the partners and the methylene groups of DAE could prevent internal dynamics.

The initial assignment of the observed experimental lines to rotational transitions was performed through a fit based on an asymmetric rigid rotor Hamiltonian, using the JB95[54] program package. Refined fits were obtained by using the AABS[55–57] program suite and a standard Watson-type Hamiltonian (A-reduction and I^r representation) by using the nonlinear least-squares fit program SPFIT developed by Pickett.[58]

Computational details

The conformational landscapes of the DAE-w, DAE-EtOH, and DAE-*t*BuOH complexes were explored by performing quantum-chemical computations. In the first step, minimum structures were determined with a conformational search by using the GFN-xTB program.[29,30] The non-redundant structures were optimized by using the B3LYP-D3(BJ) dispersion-corrected density functional combination and the def2-TZVP basis set. The energy values presented herein are zero-point vibrational energy (ZPVE) corrected relative energies. The three-body correction was not considered for these calculations. Structure optimizations and frequency computations were performed within the harmonic approximation by using the ORCA program package.[59,60]

The lowest-energy complexes optimized at the B3LYP-D3(BJ)/def2-TZVP level of theory were used as inputs for the SAPT(0)/jun-cc-pVDZ[49] computations and the NCI plots.[48] The structures of the DME (1w, EtOH$_g$, and EtOH$_t$) complexes were taken from ref. [41] and re-optimized at the B3LYP-D3(BJ)/def2-TZVP level of theory. The SAPT analysis was carried out by using the PSI4 package.[61]

Acknowledgments

Conflict of interest

The authors declare no conflict of interest.

[1] M. F. Chaplin, *Water's Hydrogen Bond Strength in Water and Life: The Unique Properties of H₂O* (Eds.: R. M. Lynden-Bell, S. Conway Morris, J. D. Barrow, J. L. Finney, C. Harper), CRC, Boca Raton **2010**, p. 69.

[2] V. Daggett, A. Fersht, *Nat. Rev. Mol. Cell Biol.* **2003**, *4*, 497–502.

[3] E. Persch, O. Dumele, F. Diederich, *Angew. Chem. Int. Ed.* **2015**, *54*, 3290–3327; *Angew. Chem.* **2015**, *127*, 3341–3382.

[4] N. O. B. Lüttschwager, T. N. Wassermann, R. A. Mata, M. A. Suhm, *Angew. Chem. Int. Ed.* **2013**, *52*, 463–466; *Angew. Chem.* **2013**, *125*, 482–485.

[5] J. P. Wagner, P. R. Schreiner, *Angew. Chem. Int. Ed.* **2015**, *54*, 12274–12296; *Angew. Chem.* **2015**, *127*, 12446–12471.

[6] P. R. Schreiner, L. V. Chernish, P. A. Gunchenko, E. Y. Tikhonchuk, H. Haus-mann, M. Serafin, S. Schlecht, J. E. P. Dahl, R. M. K. Carlson, A. A. Fokin, *Nature* **2011**, *477*, 308–311.

[7] A. A. Fokin, L. V. Chernish, P. A. Gunchenko, E. Y. Tikhonchuk, H. Haus-mann, M. Serafin, J. E. P. Dahl, R. M. K. Carlson, P. R. Schreiner, *J. Am. Chem. Soc.* **2012**, *134*, 13641–13650.

[8] G. Karir, N. O. B. Lüttschwager, M. A. Suhm, *Phys. Chem. Chem. Phys.* **2019**, *21*, 7831–7840.

[9] J. Altnöder, S. Oswald, M. A. Suhm, *J. Phys. Chem. A* **2014**, *118*, 3266–3279.

[10] R. Medel, M. Heger, M. A. Suhm, *J. Phys. Chem. A* **2015**, *119*, 1723–1730.

[11] M. Becucci, S. Melandri, *Chem. Rev.* **2016**, *116*, 5014–5037.

[12] M. Juanes, R. T. Saragi, W. Caminati, A. Lesarri, *Chem. Eur. J.* **2019**, *25*, 11402–11411.

[13] R. Medel, C. Stelbrink, M. A. Suhm, *Angew. Chem. Int. Ed.* **2019**, *58*, 8177–8181; *Angew. Chem.* **2019**, *131*, 8261–8265.

[14] F. Dietrich, D. Bernhard, M. Fatima, C. Pérez, M. Schnell, M. Gerhards, *Angew. Chem. Int. Ed.* **2018**, *57*, 9534–9537; *Angew. Chem.* **2018**, *130*, 9678–9682.

[15] D. Bernhard, M. Fatima, A. Poblotzki, A. L. Steber, C. Pérez, M. A. Suhm, M. Schnell, *Phys. Chem. Chem. Phys.* **2019**, *21*, 16032–16046.

[16] A. J. Stone, *The Theory of Intermolecular Forces*, Clarendon, Oxford **1997**.

[17] M. Fatima, A. L. Steber, A. Poblotzki, C. Pérez, S. Zinn, M. Schnell, *Angew. Chem. Int. Ed.* **2019**, *58*, 3108–3113; *Angew. Chem.* **2019**, *131*, 3140–3145.

[18] S. Grimme, R. Huenerbein, S. Ehrlich, *ChemPhysChem* **2011**, *12*, 1258–1261.

[19] G. G. Brown, B. C. Dian, K. O. Douglass, S. M. Geyer, S. T. Shipman, B. H. Pate, *Rev. Sci. Instrum.* **2008**, *79*, 053103.

[20] D. Schmitz, V. Alvin Shubert, T. Betz, M. Schnell, *J. Mol. Spectrosc.* **2012**, *280*, 77–84.

[21] W. Gordy, R. L. Cook, *Microwave Molecular Spectra, Vol. 11*, Wiley Inter-science, New York, **1984**.

[22] S. R. Domingos, C. Pérez, C. Medcraft, P. Pinacho, M. Schnell, *Phys. Chem. Chem. Phys.* **2016**, *18*, 16682–16689.

[23] I. Uriarte, S. Melandri, A. Maris, C. Calabrese, E. J. Cocinero, *J. Phys. Chem. Lett.* **2018**, *9*, 1497–1502.

[24] A. Simão, C. Cabezas, I. León, E. R. Alonso, S. Mata, J. L. Alonso, *Phys. Chem. Chem. Phys.* **2019**, *21*, 4155–4161.

[25] J. Kraitchman, *Am. J. Phys.* **1953**, *21*, 17–24.

[26] Z. Kisiel, *J. Mol. Spectrosc.* **2003**, *218*, 58–67.

[27] H. D. Rudolph, *Struct. Chem.* **1991**, *2*, 581–588.

[28] J. K. G. Watson, A. Roytburg, W. Ulrich, *J. Mol. Spectrosc.* **1999**, *196*, 102–119.

[29] S. Grimme, C. Bannwarth, P. Shushkov, *J. Chem. Theory Comput.* **2017**, *13*, 1989–2009.

[30] C. Bannwarth, S. Ehlert, S. Grimme, *J. Chem. Theory Comput.* **2019**, *15*, 1652–1671.

[31] F. N. Keutsch, R. Saykally, *Proc. Natl. Acad. Sci. USA* **2001**, *98*, 10533–10540.

[32] A. L. Steber, C. Pérez, B. Temelso, G. C. Shields, A. M. Rijs, B. H. Pate, Z. Kisiel, M. Schnell, *J. Phys. Chem. Lett.* **2017**, *8*, 5744–5750.

[33] J. C. López, R. Sánchez, S. Blanco, J. L. Alonso, *Phys. Chem. Chem. Phys.* **2015**, *17*, 2054–2066.

[34] S. Blanco, P. Pinacho, J. C. López, *Angew. Chem. Int. Ed.* **2016**, *55*, 9331–9335; *Angew. Chem.* **2016**, *128*, 9477–9481.

[35] C. Pérez, A. Krin, A. L. Steber, J. C. López, Z. Kisiel, M. Schnell, *J. Phys. Chem. Lett.* **2016**, *7*, 154–160.

[36] C. Pérez, J. L. Neill, M. T. Muckle, D. P. Zaleski, I. Peña, J. C. López, J. L. Alonso, B. H. Pate, *Angew. Chem. Int. Ed.* **2015**, *54*, 979–982; *Angew. Chem.* **2015**, *127*, 993–996.

[37] T. R. Dyke, J. S. Muenter, *J. Chem. Phys.* **1974**, *60*, 2929–2930.

[38] J. C. Pearson, K. V. L. N. Sastry, E. Herbst, F. C. De Lucia, *J. Mol. Spectrosc.* **1996**, *175*, 246–261.

[39] N. Borho, Y. Xu, *Phys. Chem. Chem. Phys.* **2007**, *9*, 4514–4520.

[40] N. Borho, Y. Xu, *Angew. Chem. Int. Ed.* **2007**, *46*, 2276–2279; *Angew. Chem.* **2007**, *119*, 2326–2329.

[41] L. Evangelisti, G. Feng, R. Rizzato, W. Caminati, *ChemPhysChem* **2011**, *12*, 1916–1920.

[42] I. A. Finneran, P. B. Carroll, M. A. Allodi, G. A. Blake, *Phys. Chem. Chem. Phys.* **2015**, *17*, 24210–24214.

[43] M. Fatima, C. Pérez, M. Schnell, 71st International Symposium on Molecular Spectroscopy, Urbana–Champaign (IL, USA), 19–26 June **2016**, Talk WC12, *Broadband Microwave Spectroscopy as a Tool to Study Dispersion Interactions in Camphor–Alcohol Systems*.

[44] D. Loru, I. Peña, M. E. Sanz, *J. Mol. Spectrosc.* **2017**, *335*, 93–101.

[45] D. Loru, I. Peña, M. E. Sanz, *Phys. Chem. Chem. Phys.* **2019**, *21*, 2938–2945.

[46] Q. Gou, L. B. Favero, G. Feng, L. Evangelisti, C. Pérez, W. Caminati, *Chem. Eur. J.* **2017**, *23*, 11119–11125.

[47] B. M. Giuliano, L. B. Favero, A. Maris, W. Caminati, *Chem. Eur. J.* **2012**, *18*, 12759–12763.

[48] E. R. Johnson, S. Keinan, P. Mori-Sánchez, J. Contreras-García, A. J. Cohen, W. Yang, *J. Am. Chem. Soc.* **2010**, *132*, 6498–6506.

[49] B. Jeziorski, R. Moszynski, K. Szalewicz, *Chem. Rev.* **1994**, *94*, 1887–1930.

[50] R. K. Crossland, K. L. J. Servis, *Org. Chem.* **1970**, *35*, 3195–3196.

[51] U. Kraatz, *Chem. Ber.* **1973**, *106*, 3095.

[52] H. Masada, F. Yamamoto, T. Okuda, *Nippon Kagaku Kaishi* **1996**, *5*, 508.

[53] C. Pérez, S. Lobsiger, N. A. Seifert, D. P. Zaleski, B. Temelso, G. C. Shields, Z. Kisiel, B. H. Pate, *Chem. Phys. Lett.* **2013**, *571*, 1–15.

[54] D. Plusquellic, JB95, available at https://www.nist.gov/pml/electromagnetics/grp05/jb95.cfm.

[55] Z. Kisiel, *Assignment and Analysis of Complex Rotational Spectra, in Spectroscopy from Space* (Eds.: J. Demaison, K. Sarka, E. A. Cohen), Kluwer, Dordrecht, **2001**, pp. 91–106.

[56] Z. Kisiel, L. Pszczółkowski, I. R. Medvedev, M. Winnewisser, F. C. De Lucia, E. Herbst, *J. Mol. Spectrosc.* **2005**, *233*, 231–243.

[57] Z. Kisiel, L. Pszczółkowski, B. J. Drouin, C. S. Brauer, S. Yu, J. C. Pearson, I. R. Medvedev, S. Fortman, C. Neese, *J. Mol. Spectrosc.* **2012**, *280*, 134–144.

[58] H. M. Pickett, *J. Mol. Spectrosc.* **1991**, *148*, 371–377.

[59] F. Neese, *Wiley Interdiscip. Rev.: Comput. Mol. Sci.* **2012**, *2*, 73–78.

[60] F. Neese, *Wiley Interdiscip. Rev.: Comput. Mol. Sci.* **2018**, *8*, e1327.

[61] R. M. Parrish, L. A. Burns, D. G. A. Smith, A. C. Simmonett, A. Eugene De-Prince, E. G. Hohenstein, U. Bozkaya, A. Y. Sokolov, R. D. Remigio, R. M. Richard, J. F. Gonthier, A. M. James, H. R. McAlexander, A. Kumar, M. Saitow, X. Wang, B. P. Pritchard, P. Verma, H. F. Schaefer, K. Patkowski, R. A. King, E. F. Valeev, F. A. Evangelista, J. M. Turney, T. D. Crawford, C. D. Sherrill, *J. Chem. Theory Comput.* **2017**, *13*, 3185–3197.